



Available online at www.sciencedirect.com

ScienceDirect

Journal of Magnesium and Alloys 11 (2023) 3130–3140



www.elsevier.com/locate/jma

Full Length Article

Achieving high ductility and strength in magnesium alloy through cryogenic-hot forming

Kai Zhang a,b,*, Zhutao Shao a, Joseph Robson C, Yan Huang d, Jinghua Zheng E, Jun Jiang a,*

^a Department of Mechanical Engineering, Imperial College London, London SW7 2AZ, UK
 ^b Department of Mechanical Engineering, University College London, London WC1E 7JE, UK
 ^c Department of Materials, The University of Manchester, Manchester M1 3BB, UK
 ^d BCAST, Institute of Materials and Manufacturing, Brunel University London, Uxbridge UB8 3PH, UK
 ^c College of Material Science and Engineering, Nanjing University of Aeronautics and Astronautics, Nanjing 211106, China
 Received 3 May 2023; received in revised form 10 September 2023; accepted 15 September 2023
 Available online 13 October 2023

Abstract

Magnesium alloys are the lightest structural alloys and have attracted substantial research attention in the past two decades. However, their mechanical properties, including ductility and strength, are limited after forming due to the formation of coarse grains and strong texture. This study proposes and proves a new cryogenic-hot forming process concept. Cryogenic deformation is imposed before the hot deformation. The effect of the cryogenic step has been compared with a conventional direct hot deformation process. The mechanical properties, microstructure, and texture of both the novel and conventional process routes have been compared. The cryogenic-hot deformed sample exhibits the highest ductility and fracture strength (ultimate tensile strength: 321 MPa, ductility: 21%) due to effective grain refinement and texture weakening by cryogenically formed twin-twin interaction induced recrystallisation. The proposed cryogenic-hot forming process can be a potential innovative manufacturing method for producing high-performance magnesium components.

© 2023 Chongqing University. Publishing services provided by Elsevier B.V. on behalf of KeAi Communications Co. Ltd. This is an open access article under the CC BY-NC-ND license (http://creativecommons.org/licenses/by-nc-nd/4.0/)
Peer review under responsibility of Chongqing University

Keywords: Magnesium alloys; Dynamic recrystallisation; Twinning; Cryogenic deformation.

1. Introduction

An innovative magnesium alloy forming method to improve ductility and strength is needed. Magnesium and its alloys attract substantial interest from researchers and industries as they are promising lightweight materials for structural applications in the automotive, aerospace and electronics industries [1–4]. However, the ductility and strength of conventional Mg alloys are limited due to their coarse grains and strong texture which are related to processing methods. Fine grains can considerably strengthen magnesium alloys [5,6], due to the Hall-Petch relationship [7]. For example, an exceptionally high strength was achieved in Mg alloy AZ31

E-mail addresses: kai.zhang17@imperial.ac.uk, kai.zhang6@outlook.com (K. Zhang), jun.jiang@imperial.ac.uk (J. Jiang).

with ultrafine grains via a low-speed extrusion [6]. However, the ductility of Mg alloys is limited by their strong texture [8]. The conventional magnesium production processes are generally time-consuming and expensive. For example, the rolling process consists of multiple passes including about 12–18 hot rolling passes [9]. It is also difficult to achieve a high strength-ductility synergy [10]. Therefore, finding a novel and effective processing technique is necessary to improve strength-ductility through grain refinement and texture weakening.

Recent work has demonstrated that exploiting twinning to provide alternative sites for recrystallisation can be effective in refining grain size and weakening the typical strong basal texture [11]. Dynamic recrystallisation (DRX) in magnesium alloys generally occurs during hot deformation processing [12]. It leads to the evolution of grain size and texture [13,14], leading towards a strong basal texture [2,15].

^{*} Corresponding authors.

Recently, evidence shows that recrystallisation near deformation twins (twin recrystallisation) during hot deformation at high strain rates could weaken the basal texture [11]. Further study on the annealing process of Mg-rare earth alloys confirmed that recrystallisation around double twins weakened the deformation texture field [16]. Twin recrystallisation and texture weakening can also contribute to the high ductility in Mg alloys [17].

Furthermore, twin recrystallisation can lead to the formation of a significantly refined grain structure by introducing a large number of nuclei for recrystallized grains [11,18]. Formation of a high-density of twins at high strain rates promoted this refinement in grain structure [11], while the effects of twins on microstructure at a low strain rate were negligible [19]. Twins were also observed in high-ratio differential speed rolling, which can contribute to the formation of fine grains [20]. In addition, the grains formed at twins can have a different texture from those formed at other sites [21]. Hence, twin recrystallisation can effectively weaken the texture and refine grains in Mg alloys.

Cryogenic deformation is an alternative more effective twinning method that avoids the expense or difficulties of adding rare earth elements or utilizing high-strain rate deformation. Since the critical resolved shear stress for twinning is less temperature-dependent compared with dislocation slip, at cryogenic temperature, twinning rather than dislocation slip tends to be activated to accommodate the imposed plastic deformation [22–25]. This point is supported by recent evidence that more twins were observed in cryogenically deformed pure titanium [26,27] and the cryo-rolled Mg alloys [23]. A cryo-forged titanium showed ultra-high strength and ductility at both room and cryogenic temperatures due to the formation of nanotwins [28]. The numerous twins in cryodeformed Mg and its alloys can contribute to their higher strain hardening rate [22,29]. The mechanical responses and deformation mechanisms including twinning and slips at cryogenic temperatures were also investigated by the visco-plastic modelling [24]. It was also found that the strength of rolled Mg alloys after cryogenic treatment increased, which could be due to the twin strengthening [30]. Furthermore, the deep cryogenic-elevated temperature cycling treatment was applied in a sand-cast Mg-6Gd-3Y-0.5Zr, and it showed an increase in strength but a decrease in elongation [4]. Although there are some studies which applied the twinning in Mg alloys with pre-deformation at room temperature [18,31], the twinning and slip mechanisms would be different at cryogenic temperature. To the best of the authors' knowledge, the study of activation of twinning but constraining dislocation movement in Mg alloys at extreme thermal conditions, *i.e.*, at cryogenic temperature, is rarely reported.

Combining cryogenic deformation with subsequent hot deformation to achieve effective twin recrystallisation has not been attempted in Mg alloys, potentially a novel effective magnesium forming technique. Also, to what extent the strength and ductility of the cryogenic-hot formed magnesium alloys can be improved through this method needs to be evaluated with some insights into the underlying mechanism.

Thus, this study aims to prove the feasibility of the concept: a cryogenic-hot forming process for magnesium alloys that can improve the mechanical properties of formed magnesium compared to the conventional cast-hot forming method. In this feasibility study, the proposed cryogenic-hot forming and conventional cast-hot forming processes were undertaken using in-lab compression tests. To understand how this novel process route works, detailed microstructural and texture analysis was performed. AZ31 (the most widely used wrought magnesium alloy) is selected in the current study as a relatively low-cost and well-accepted material that may be amenable to the novel process route.

2. Methodology

2.1. Material and experimental tests

An as-cast AZ31 alloy (Mg-Al-Zn alloys class) ingot was received and machined into testing cubic-shaped samples ($10~\text{mm} \times 10~\text{mm} \times 10~\text{mm}$). These samples were processed using various thermal-mechanical pathways. These pathways are shown schematically in Fig. 1(a). The samples were firstly compressed at cryogenic temperature (CT, $-196~^\circ\text{C}$) to a designed strain of 0.08 before fracture, using an Instron 5584 machine, as abundant twins are proposed to occur at a low temperature. The samples were immersed in a liquid nitrogen container within an environmental chamber during

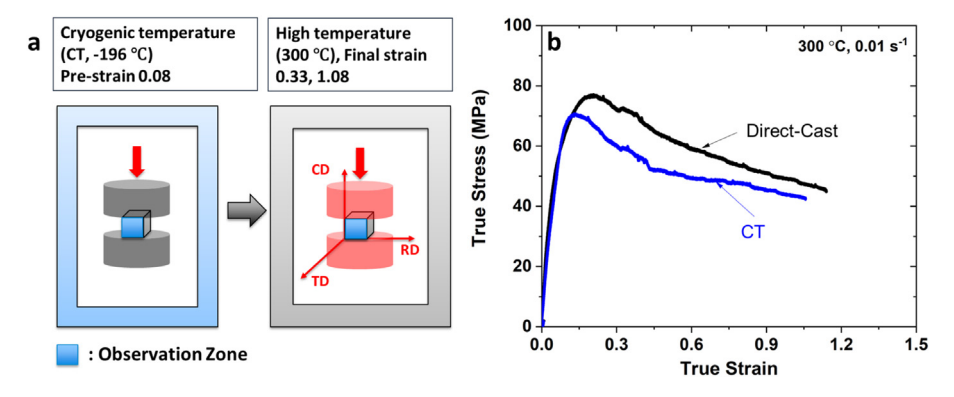


Fig. 1. (a) A schematic diagram showing the experimental compression procedures: pre-compression at cryogenic temperature (CT) and the subsequent hot deformation (HD). (b) The flow stress curves of the direct-cast and CT-deformed samples deformed at 300 °C, 0.01 s⁻¹.

CT compression to maintain the deformation temperature at −196 °C. Both CT deformed and as-cast samples were then subjected to uniaxial hot compression. The hot compression was conducted using Gleeble 3800 at a deformation temperature of 300 °C and a strain rate of 0.01 s⁻¹. The heating rate is set as 5 °C/s and the holding time is 60 s to maintain accurate temperature control before the hot compression. A pair of thermo-couples was welded to the centre of the specimen surface to measure and monitor the temperature and provide feedback signals to the temperature control system to maintain the test at the designed temperature. The compression test was conducted to two plastic strain levels of 0.33 and 1.08, which provides insights into the microstructure evolution during the hot compression in the middle and late stages. The total strain of direct-hot and cryogenic-hot compressions remained the same to compare their microstructures and mechanical properties. Both cryogenic and hot compression tests are uniaxial to keep the deformation path consistent in these deformed samples. To preserve the as-hot-deformed microstructure, an air quench was applied immediately onto the hot deformed samples at the end of the test.

Fig. 1(b) plots the true flow stress-strain curves during the Gleeble test of the direct-cast and cryogenic-temperature (CT)-deformed samples at 300 °C, 0.01 s⁻¹, respectively. All flow stresses show an initial increase and a subsequent decrease with increasing deformation, indicating a continuous softening occurrence at the late stage of the hot compression test, which could be attributed to dynamic recrystallisation. The softening in the CT-HD sample during the hot deformation process is more significant after its lower peak stress. This could be due to the more accumulated stored energy in the CT-deformed sample to promote recrystallization in the hot deformation [13,32].

Tensile tests at room temperature were conducted to evaluate the mechanical properties of the hot compressed samples. Since the size of these samples has been compressed to the same final strain level of 1.08, it is challenging to machine out standard tensile testing samples. Thus, small tensile specimens with gauge dimensions of 5 mm \times 2 mm \times 0.5 mm were machined along the central part of the compressed samples. The tensile tests were carried out using a Deben micromechanical tensile test machine using a 0.2 mm/min crosshead speed. Three tests were conducted for each condition to ensure the repeatability of the results. As the micro-tensile tests are non-standard, the machine compliance may affect the Young's modulus measurement, while all the samples underwent the same testing conditions, making the data internally consistent and useful for drawing relative conclusions. The strength and ductility of the as-cast and direct-hot samples are measured as the benchmark, which are consistent with the reference [33].

2.2. Microstructure characterisation

The as-received and hot compressed samples were prepared for EBSD microstructure characterisation by progressively grinding from 2500 to 4000 grit SiC paper for ~ 5 min

and then polishing with oxide polishing suspension for ${\sim}15$ min to achieve mirror-finishing. The EBSD maps were acquired from a Hitachi 3400 scanning electron microscope (SEM) equipped with a Bruker e-Flash, Quantax Esprit 2.1 system. The operating voltage of the SEM is set at 25 kV to achieve optimal imaging quality. Scanning step sizes of 1.5 μm and 3 μm were selected to scan the recrystallised (hot deformed) and none recrystallised (pre-deformed) samples, respectively, because of the initial large cast grains and recrystallised refined grains. To obtain more detailed information from selected regions of interest, a 0.8 μm step size was selected.

The analyses of EBSD data were undertaken using HKL CHANNEL 5 software. The kernel average misorientation (KAM) value was calculated based on the average misorientation between each pixel and its surrounding 5×5 pixels. The measured KAM values indicate a geometrically necessary dislocation (GND) density [34]. The subset figures were plotted using the subset components in HKL software. The average grain size was weighed by area fraction and included boundary grains. The texture was plotted with pole figures, and in texture analysis the fine-grained zone is defined as the grains whose size is smaller than 25 μ m. In EBSD IPF maps and pole figures, CD is applied to represent the compression direction, and RD represents the direction perpendicular to CD.

3. Results

3.1. Mechanical behaviours of the hot deformed Mg alloy AZ31

The overview of true tensile stress-strain curves of all samples is presented in Fig. 2. The cryogenic deformation step can be seen to strongly affect the mechanical properties in these AZ31 samples. For the initial as-cast sample (green line in Fig. 2), the elongation to failure, EL, 0.2% proof stress (yield strength, YS), and fracture strength (FS) are 15%, 56 MPa and 211 MPa, respectively. The material was strengthened after the direct hot compression at 300 °C

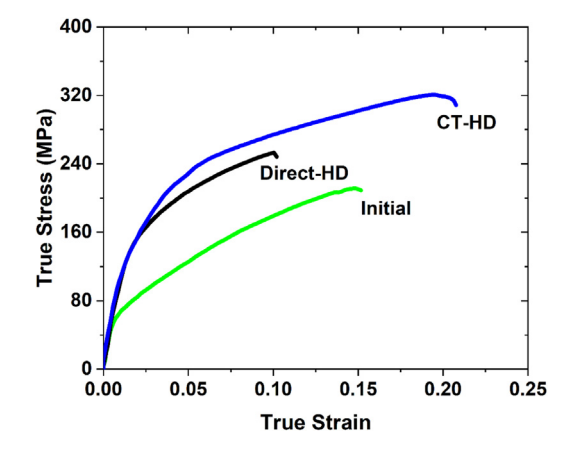


Fig. 2. The true stress-strain tensile curves for the initial, direct-HD and CT-HD samples.

(direct-HD), but the ductility was compromised. As seen in the black line (Fig. 2), the YS and FS increase from 56 and 211 MPa to 92 and 253 MPa, respectively, but their EL decreases from 15% to 10%. However, this typical strengthductility trade-off is eliminated by imposing cryogenic-hot deformation (CT-HD sample, blue line); the sample shows a significant boost in both the strength and elongation to failure compared to the as-cast and the directly hot deformed materials. For example, the highest yield, fracture strength and elongation to failure have been achieved in the CT-HD material, i.e., 111, 321 MPa and 21%, respectively, which corresponds to $\sim 100\%$ increase in yield strength and $\sim 50\%$ increase in fracture strength and elongation to failure, compared to the initial as-cast sample, or ~110% increase in elongation to failure and ~33% increase in fracture strength if we compare with the directly hot deformed one. The CT-HD AZ31 sample also shows superior mechanical properties, compared to commercial AZ31 rolled sheets with fracture strength of 263 MPa and elongation to failure of 16% in the rolling direction [35].

3.2. Microstructural behaviours in the hot-deformed samples

The cryogenic-hot deformation significantly enhances the level of grain refinement. The microstructural behaviours of these hot-deformed samples with a final strain of 1.08 were analysed to explain the mechanical behaviours in Fig. 2. The inverse pole figure (IPF) maps of these samples are plotted in Fig. 3. The IPF map of the initial sample is plotted in Fig. 3(a), and it shows the typical homogenous as-cast

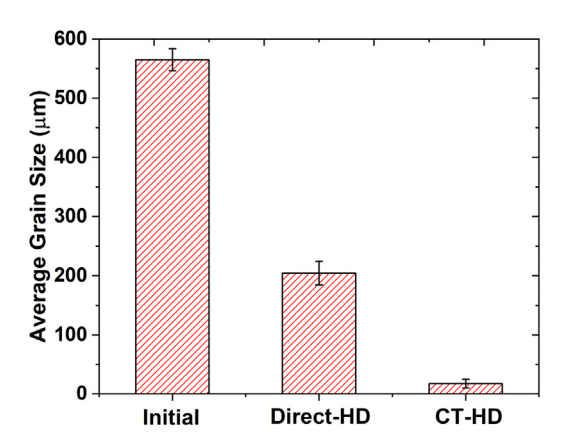


Fig. 4. Average grain size in the initial, direct-HD and CT-HD samples.

microstructure with coarse grains. Fig. 3(b) shows the microstructure of the direct-HD sample, which is rather inhomogeneous with some coarse grains mixed with refined grains. However, the cryogenic-hot deformed sample exhibits a considerably finer grain size than those in the direct-HD sample, as shown in Fig. 3(b) and (c). These results indicate that predeformation at CT can significantly enhance the grain refinement that occurs in the subsequent hot deformation process.

The grain refinement is more effective in the cryogenichot deformed sample than in the directly hot deformed condition. Based on the EBSD maps shown in Fig. 3, the average grain sizes of these samples are statistically analysed and plotted in Fig. 4. The average grain size of the initial sample is

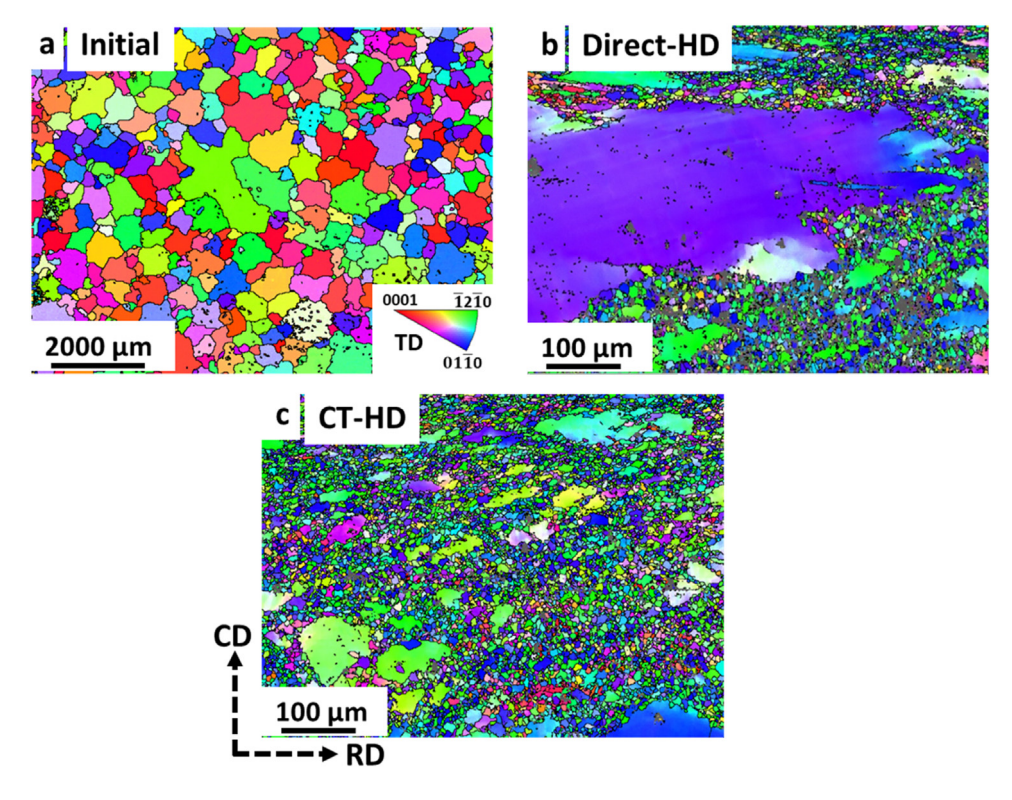


Fig. 3. EBSD IPF maps of (a) the initial as-cast sample, and (b-c) the hot-deformed samples at 300 °C to a final strain of 1.08, (b) directly hot-deformed (direct-HD) one, and (c) CT-hot-deformed (CT-HD) sample.

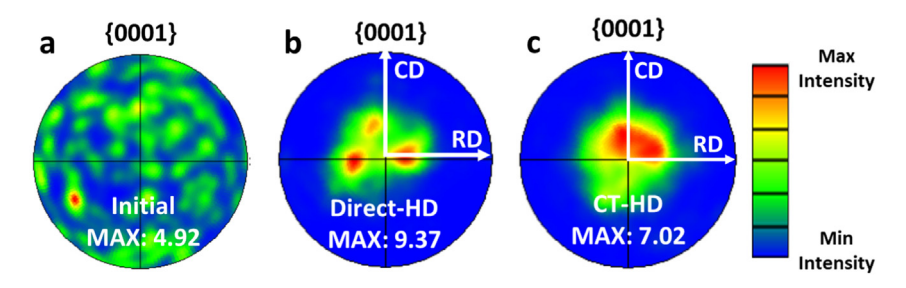


Fig. 5. {0001} pole figures of (a) initial sample, (b) direct-HD sample and (c) CT-HD sample in fine-grained zones. The unit of the colour bar is in multiples of a uniform distribution (mud).

565 µm. This has been reduced through direct hot deformation, for which the measured grain size is 205 µm. However, compared to the direct hot deformed one, the cryogenic-HD deformation shows remarked grain refinement with an average grain size of 17 µm, which is reduced by more than thirty-three times compared to the initial sample. The cryogenic deformation is therefore effective in promoting grain refinement. The error bar in Fig. 4 was calculated by the standard error of the grain size distribution, and the shorter error bar in the CT-HD sample indicates that the grain size distribution of the CT-HD sample is more homogenous than the direct-HD sample. Furthermore, the direct-HD condition contains some remnant very large grains. The grain size distribution of these hot-deformed samples is shown in Supplementary Fig. A.1, and it is found that more coarse grains are observed in the direct-HD sample, while the fine grains dominate in the cryogenic-hot deformed sample. This fine-grained and homogenous microstructure would be one of the main reasons for the high strength and ductility of the cryogenichot deformed sample, as shown in Fig. 2.

In addition to refining the grains and reducing the occurrence of some very large grains, the CT-HD process path potentially weakens the texture that results after the hot deformation process. Apart from grain size, the strong basal texture formed in magnesium alloys is another main reason for poor ductility in certain loading orientations.

Texture analysis was conducted, and the corresponding {0001} pole figures in fine-grained zones of initial, direct-HD and CT-HD samples are plotted in Fig. 5 to exclude the coarse grain effect on texture. As the initial sample is an as-cast alloy, its texture is random and weak (Fig. 5(a)). However, once the material is hot-deformed, a strong texture is generated, e.g., the direct-HD sample in fine-grained zones shows the strongest texture with a maximum intensity of 9.37 mud in Fig. 5(b). The weakest hot deformed texture is found in the cryogenic-hot deformed sample with the texture intensity of 7.02 mud, as seen in Fig. 5(c). It suggests that the cryogenic deformation weakens the texture that arises from the hot deformation process. The weaker texture in the cryogenic-temperature (CT)-HD sample would contribute to its higher elongation to failure (Fig. 2). In addition, the {0001} pole figures in whole zones of these hotdeformed samples are shown in Supplementary Fig. A.2. It is also found that the cryogenic-hot deformed sample shows a weaker texture. The differences in texture formation and grain refinement in these hot-deformed samples are generated during their recrystallisation in the hot-deformation processes, which will be revealed and analysed in-depth in the following section.

3.3. Microstructural evolution during cryogenic deformation and subsequent dynamic recrystallisation

High dislocation densities are found near the twin boundaries and twin-twin interactions. An in-depth microstructure analysis is conducted to shed more light on the deformation process and recrystallisation mechanism in this cryogenic-hot process, as shown in Figs. 6–8. As discussed in the previous section, the CT-deformed sample after hot deformation shows a more homogenous microstructure with refined grains and a weaker texture compared with the directly hot-deformed case. The comparison of grain orientation change for the same region of interest before and post the cryogenic deformation is shown in Fig. 6. The initial as-cast sample is shown in Fig. 6(a), and its KAM value is very low with a relatively homogenous distribution (Fig. 6(c)).

On the contrary, after deformation at CT, abundant twin boundaries, especially (1012)-(0112) twin-twin interactions, are observed. Grain A is selected to highlight the twinning behaviour during the cryogenic deformation, as presented in Fig. 7. Two tension twin variants, A2 and A3, are generated in the matrix AM1 to form (1012)-(0112) twin-twin interactions and almost the entire grain A is consumed by these two twin variants. These two twin variants, A2 and A3, show different orientations and are located away from the centre of the {0001} pole figure, contributing to weakening the texture. In addition, the KAM value is high around these twin boundaries, especially the interacting twin boundaries, indicating that the dislocation density is high in these sites, as shown in Figs. 6(d) and 7. These high dislocation density sites would be the preferential recrystallised sites and enhance the recrystallisation in the subsequent hot deformation process.

The profound recrystallisation near twin boundaries and twin-twin interactions results in a more homogenous microstructure and refined grains. The microstructure analysis of the cryogenically deformed sample during the subsequent hot compression process at 300 °C is shown in Fig. 8. As shown in Fig. 8(a) and (b), at the final deformation strain of 0.33, some recrystallised grains with fine structures are observed

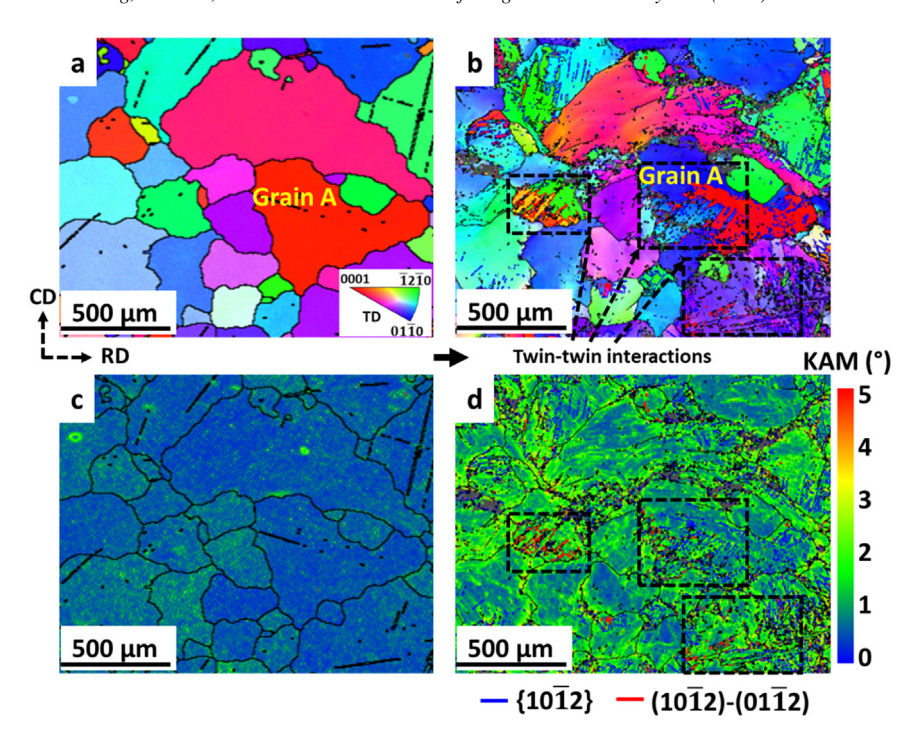


Fig. 6. IPF maps of (a) the initial Mg alloy AZ31 sample and (b) the CT-deformed sample to a strain of 0.08, and the corresponding KAM maps of (c) the initial Mg alloy AZ31 sample and (d) the CT-deformed sample, respectively.

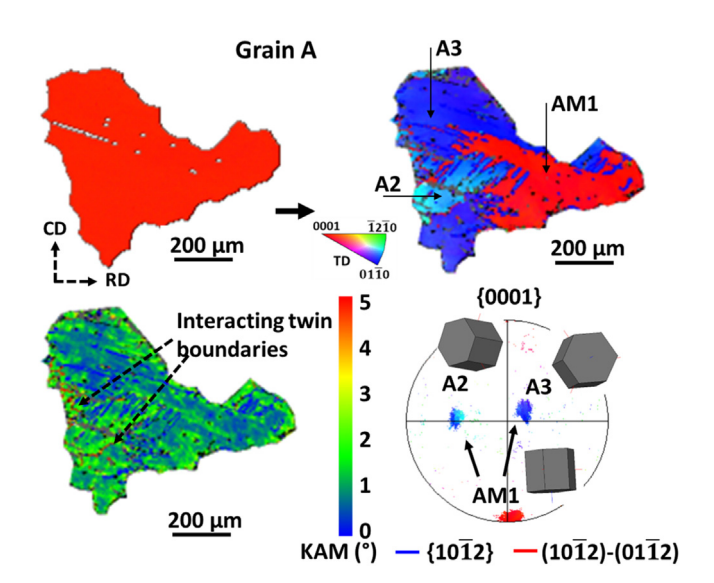


Fig. 7. IPF map, KAM map and orientation evolution in grain A of CT-deformed sample in Fig. 6, respectively.

and mainly located around the twin boundaries, especially the boundaries of (1012)-(0112) twin-twin interactions. According to its KAM map in Fig. 8(c), the KAM value is high near some remaining twin boundaries, which could become the recrystallisation sites and contribute to further recrystallisation. Therefore, the twins and twin-twin interactions in the cryogenically deformed sample provide excellent sites for active dynamic recrystallisation during the hot deformation process. The dynamic recrystallisation can form the homogenous microstructure and refined grains in Fig. 3(d).

The dynamic recrystallisation around twin-twin interactions is pronounced, resulting in texture weakening and grain refinement. The typical zone (B in Fig. 8(a)) is selected to analyse the recrystallisation mechanisms in the CT-deformed sample. As shown in Fig. 8(d), abundant recrystallised grains are located in the regions that show elongated shapes similar to those of the twin bands and are bounded by matrix grains of identical orientations. Although the character of twin boundaries is lost after dynamic recrystallisation, the misorientations between the recrystallised grains and their neighbour matrix grains still share the [1120] axis or the [0110] axis or their equivalent axes. The results indicate that these recrystallised grains are generated around the boundaries of (1012)-(0112) twin-twin interactions, as these twin-twin interactions are formed by two {1012} tension twins (TTWs) and share the $[11\bar{2}0]$ axis or the $[01\bar{1}0]$ axis. In Fig. 8(e), the orientations of these recrystallised grains, such as grains B1, B2 and B3, are discrete and different from the orientation of the matrix BM, which would contribute to the formation of a broad and weak texture. The various orientations would also promote the activation of dislocation slips and result in dislocation accumulations near the boundaries. According to Fig. 8(f), the KAM value is high near the boundaries, promoting further recrystallisation during the hot deformation pro-

3.4. Microstructures in the hot deformation process for the direct-HD samples

Deformation bands are the preferential sites for recrystallisation in the direct-HD sample. A microstructural

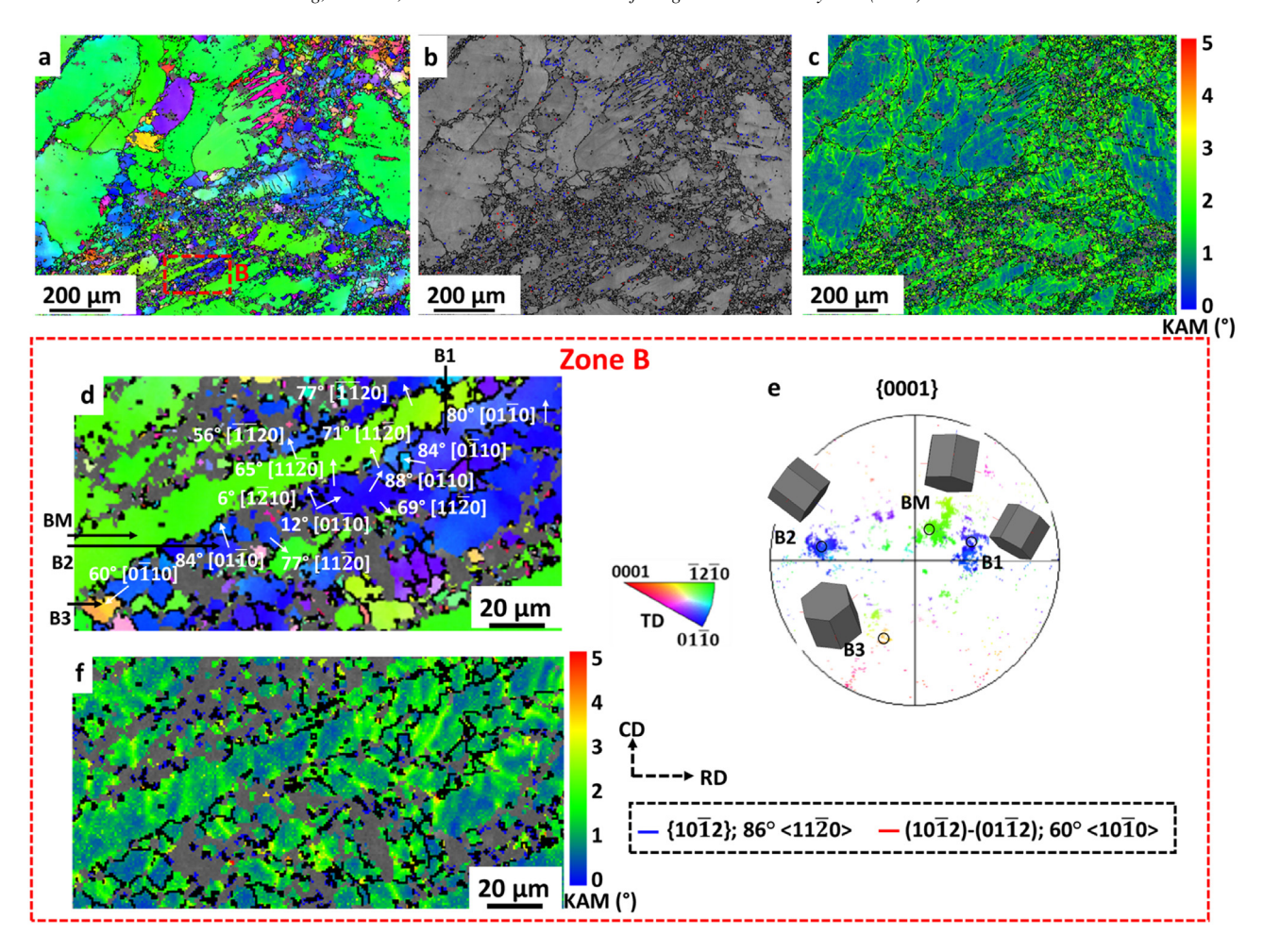


Fig. 8. (a) IPF map, (b) band contrast map with twin boundaries, and (c) KAM map in the CT-HD sample with a final strain of 0.33. (d) IPF map, (e) {0001} pole figure, and (f) KAM map in Zone B of this sample, respectively.

analysis of the direct-HD sample with a total strain of 0.33 was conducted to study the dynamic recrystallisation behaviours. Fig. 9(a-c) shows the IPF map, the band contrast map with twin boundaries, and the KAM map of the direct-HD sample. This sample has a low recrystallised area fraction, and the dynamic recrystallisation mainly occurs around the deformation bands, including the deformed areas near grain boundaries. To observe more details, Fig. 9(d-1) plots the IPF maps, the band contrast maps, and the KAM maps of three typical zones in this area. The central recrystallisation region in this sample is around deformation bands, as shown in Fig. 9(d), (g) and (j). Abundant recrystallised grains are refined and located around the deformation bands in Zone C, while almost no recrystallisation occurs in the regions away from the deformation bands. This could be attributed to the high KAM value around the narrow region of deformation bands, accumulating abundant dislocations and sufficient stored energy to promote recrystallisation. In Fig. 9(e) and (h), TTWs are observed in Zone D and show the coarse structure. According to Fig. 9(k), some sites with high KAM values spread in the twin variant D1 and show the 'string-like' feature from one twin boundary to another twin boundary. In Fig. 9(f), (i) and (l), the compression twins (CTWs) also show the coarse structure, and few sites with high KAM values are distributed in the twin variant E1. However, no recrystallised grains are observed around these TTWs or CTWs. Furthermore, in Zone F shown in Supplementary Fig. A.3. (a-c), most recrystallized grains are located in deformation bands and KAM values are low in these recrystallised grains, while almost no recrystallisation occurs near the twin boundaries. These results indicate that deformation bands are the preferential sites for recrystallisation in the direct-HD sample.

4. Discussion

4.1. Recrystallisation near twins in the CT-HD sample during hot deformation

The high twinning and twin-twin interaction activity would be attributed to limited dislocation slip and high local stress during cryogenic deformation. The high activity of twin nucleation leads to abundant twin variants, which interact to form twin-twin interactions. This profoundly influences the microstructural evolution during the subsequent hot deformation step.

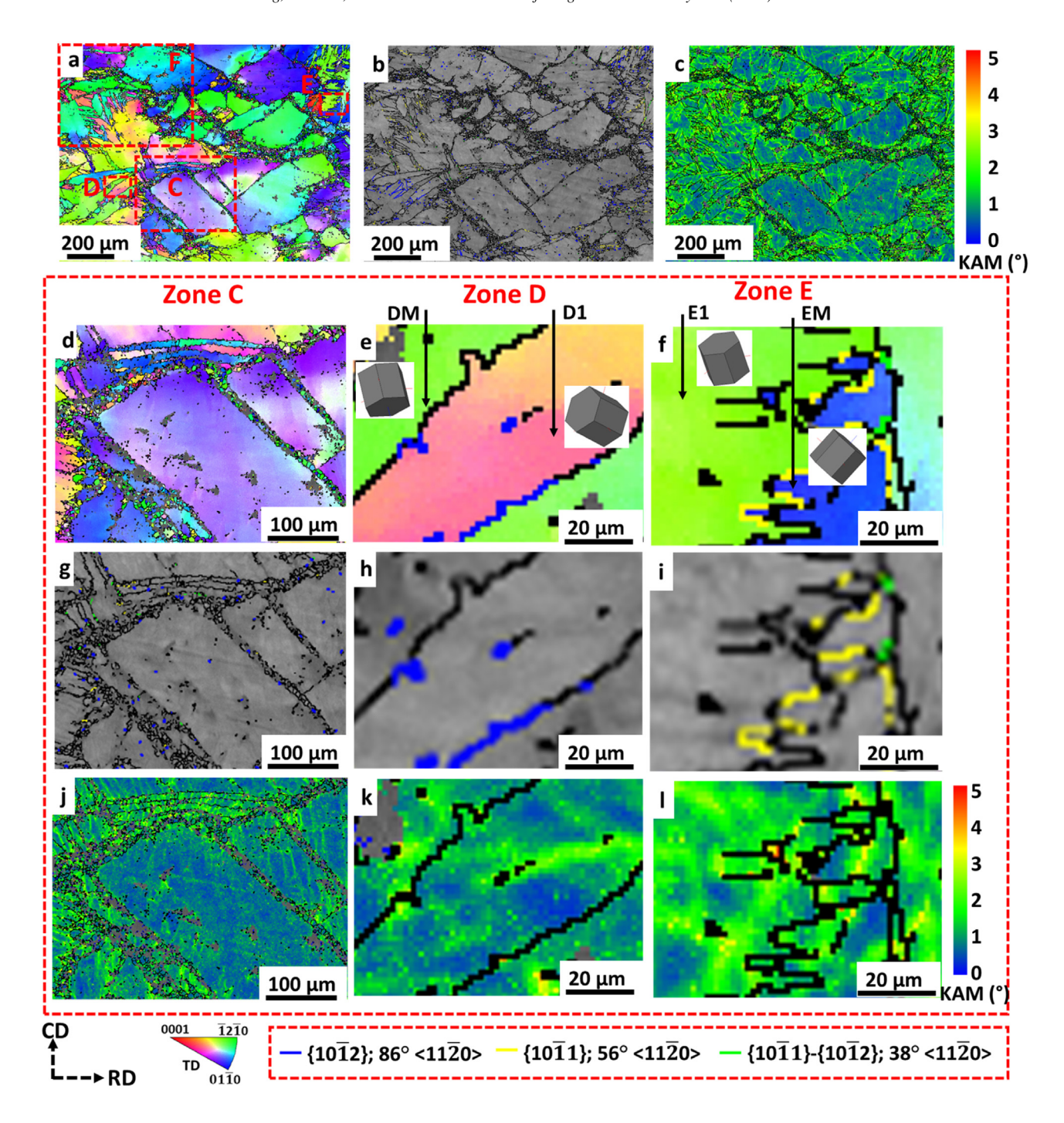


Fig. 9. (a) IPF map, (b) band contrast map with twin boundaries, and (c) KAM map in the direct-HD sample with the final strain of 0.33. (d-f) IPF maps and corresponding, (g-i) band contrast maps with twin boundaries, and (j-l) KAM maps in Zone C, Zone D and Zone E, respectively.

As shown in Figs. 6 and 7, abundant twins, especially (1012)-(0112) twin-twin interactions, are generated in the cryogenic-temperature (CT)-deformed sample. The result is consistent with active twinning behaviours in the cryogenic deformation in the Mg alloys [22]. The high twinning and twin-twin interaction activity are due to the difficulty activating dislocation slip and high local stress during cryogenic deformation, as discussed in detail elsewhere [22,23]. The restricted slip activity leads to the development of high local

stress near the grain boundaries, resulting in enhanced twin nucleation, as twin nucleation generally requires considerable stress [36].

The high KAM values due to twin-twin interactions have two main sources. Firstly, as another twin variant will prevent twin propagation in twin-twin interactions, the fine structures of twin-twin interactions can block the dislocation slips effectively and result in high KAM values, according to the boundary-strengthening effects. One twin is blocked by another, and the dislocations around the twin tip due to local plastic relaxation become trapped [37]. Secondly, twin-twin interactions themselves produce more orientations, some of which will be favourable for, further promoting dislocation accumulation

Twinning-induced dynamic recrystallisation around twintwin interactions plays a vital role in achieving refined grains and weak texture. The high KAM values close to the twintwin interactions reflect the high local stored energy, providing the driving force for recrystallisation at the twin-twin interactions. In Fig. 8, during the early stage of dynamic recrystallisation, many new grains can be seen to nucleate at the twin-twin interactions, resulting in significant grain refinement. The characteristics of the twin boundaries remain, indicating that the dynamic recrystallisation does not change the twin relationship [13,14]. As the orientations of recrystallised grains in these twin-twin interactions are diversified, this leads to a weaker and wider texture spread in the cryogenic-temperature CT-HD sample. Therefore, in the hot deformation process of the CT-HD sample, active twinninginduced dynamic recrystallisation around abundant twin-twin interactions plays a vital role in achieving refined grains and a soft texture, although the twin volume fraction can be limited to some extent.

The recrystallization temperature of Mg alloys could only occur above about 200 °C when the deformation strain is low and <0.1, and it can also take about 700 s to initiate recrystallisation at 400 °C [38]. The processing temperature of 300 °C during the hot deformation is close to the recrystallisation temperature, and it should take at least 700 s to initiate recrystallisation at 300 °C. The heating rate of 5 °C/s is high and the holding time of 60 s is short, so the heating and holding process before the hot deformation should have very limited recrystallisation and negligible effect on microstructure evolution.

4.2. Recrystallisation in the direct-HD samples during hot deformation

The recrystallisation in the direct-HD sample mainly occurs around the deformation bands, including the deformed areas near the grain boundaries, as shown in Fig. 9. This could be attributed to the narrow structure of deformation bands in which abundant dislocations accumulate to activate recrystallisation, which is expected behaviour for deformed magnesium. The formation of deformation bands in the direct-HD sample would be attributed to its more dislocations, limited twin recrystallisation sites and more inhomogeneous deformation [23,39], while more twins and more homogenous twin recrystallisation in the CT-HD sample can contribute to its more homogenous deformation and significant grain refinement. In addition, more CTWs in the direct-HD sample indicate its inhomogeneous deformation and strain concentration in these regions as they generally require high stress to be activated, and CTWs are also related to the formation of deformation bands [40,41]. However, compared to abundant twin boundaries in the CT-HD sample, the density of deformation bands in the direct-HD sample is limited, resulting in a low recrystallised area fraction and therefore no effective refinement of the grain structure. Unlike twin recrystallisation, recrystallisation near deformation bands and grain boundaries generally contributes to texture strengthening in Mg alloy AZ31. This could be attributed to orientated basal grain growth [15,39].

Recrystallisation at twins is rarely observed in the direct-HD sample during the early stage of hot deformation, as shown in Fig. 9. Almost no recrystallisation is observed around the boundaries of TTWs and CTWs. Unlike the twintwin interactions in the CT sample, the KAM values are generally low in most areas of TTWs and CTWs and spread around these twins, indicating a reduced local stored energy for recrystallisation. Note that most of the plastic relaxation during twinning takes place in the region infront of the twin tip. When the twin is able to grow fully across a grain, the dislocations generated by this relaxation can be dissipated. When the twin is blocked (due to a twin-twin interaction as frequently observed in the CT case), these dislocations are trapped inside the grain. For the direct-HD case, recrystallisation at twins therefore does not make a significant contribution to reducing the grain size or spreading the texture. As the deformation strain and path can change the microstructures, the total strain and uniaxial deformation path in the direct-HD and CT-HD samples were kept the same to compare their main microstructure difference. As shown in Figs. 6–9 and according to the reference [22,23], unlike the deformation bands and few twins in the direct-HD sample, the main microstructure in the CT-HD sample is the twin-twin interactions with high dislocation density near twin boundaries, which provide main sites for recrystallisation. This also explains why there is more active recrystallisation near twins in the CT-HD sample (in Fig. 8) than that in the direct-HD sample (in Fig. 9).

4.3. Enhancement of elongation to failure and strength in the hot-deformed sample with cryogenic pre-deformation

The smaller, more uniform grains, and the weaker texture in the cryogenic-hot deformed sample are both suggested to be the reason for the improved strength and ductility, compared to the initial as-cast and direct-hot deformed samples. The strength of Mg alloy AZ31 generally increased with decreasing grain size, as suggested by the Hall-Petch hardening relationship. Furthermore, the ductility of Mg alloys generally increases with decreasing grain size [8] due to the limited twins and enhanced non-basal slip in the fine-grained sample [5]. Dislocation slip rather than twinning generally dominates the deformation as the grain size reduces [42], as grain boundaries have more significant strengthening effects on twinning than dislocation slip. The limited twins formed during tensile testing of the fine-grain sample can be beneficial because certain twinning behaviours, such as the formation of {1011}-{1012} double twins, are generally associated with fractures [43]. The texture is also critical to the elongation to failure achieved in magnesium alloys. As shown in Fig. 5, the weakest texture was formed in the cryogenichot deformed sample, which would result in more randomly

orientated grains to activate dislocation slip more easily [8], thus improving the ductility. The strength of the direct-HD sample is higher than that of the initial cast sample, this can be related to the refined grains in the direct-HD sample. While the ductility of the initial cast sample is higher than that of the direct-HD sample, this can be attributed to the random texture of the initial cast sample which can provide more various paths for slip activation. However, the ductility of the initial cast sample is lower than the cryogenic-hot deformed sample, although the texture of the initial cast sample is weaker. This could be attributed to the coarse grain size of the initial cast sample. It is generally easy to activate basal slips and twins in the deformation of the coarse-grained cast sample [44], which can result in strain localisation and inhomogeneous deformation, thus generating cracks and fracture near these sites to reduce the ductility. In the fine-grained cryogenic-hot sample, non-basal slips including pyramidal slips can be activated to accommodate the more homogenous deformation for its enhanced plasticity [5,45].

Grain size and texture are the main factors which affect the mechanical properties of Mg alloys, as their poor strength and ductility are generally related to coarse grains and strong texture [6,11]. The aim of this pilot study is to demonstrate a new methodology to improve the strength and ductility of Mg by modifying their texture and grain size through a twinning-driven DRX process. Practical issues are expected and could be addressed in a later stage, for example, cryogenic hot rolling could be applied to achieve more homogeneous microstructure and mechanical distribution. In addition, compared to conventional manufacturing methods with low efficiency and high cost, such as the rolling process consisting of 12–18 hot passes [9], our study provides a cost-effective method to achieve high-performance Mg alloys.

5. Conclusions

Cryogenic-hot compression has been imposed on AZ31 samples to check its feasibility as a new magnesium-forming method. The tensile properties have been assessed and compared with direct cast-hot compressed and as-cast samples. The underlying microstructure evolution before and post cryogenic deformation and during the hot compression has been revealed and analysed. The following conclusions can be drawn:

- (1) The proposed cryogenic-hot deformation process significantly enhanced the ductility and fracture strength of the samples by 110% and 33%, respectively, compared to the direct cast-hot deformed sample.
- (2) The proposed cryogenic-hot deformation process effectively refined the grain size and weakened the texture. The grain size has reduced from 565 μm to 17 μm with a homogenous microstructure, and the texture was weakened to 7.02 mud, compared to the direct-hot-deformed sample.
- (3) The reasons for significant grain refinement and texture weakening have been found to be the abundant

- twins, especially twin-twin interactions, generated during the cryogenic deformation. These twin-twin interactions with high stored energy in the CT-deformed sample provided great sites for active recrystallisation during the hot compression.
- (4) Deformation bands with high stored energy have been identified as the main recrystallisation sites in the casthot deformed samples. Regions near TTWs, due to the low stored energy, did not show active recrystallisation.

Data availability

The raw/processed data required to reproduce these findings cannot be shared as the data also forms part of an ongoing study.

Declaration of Competing Interest

The authors declare that they have no known competing financial interests or personal relationships that could have appeared to influence the work reported in this paper.

Acknowledgments

We are grateful for the financial support from the President's PhD Scholarship of Imperial College London. The authors would like to thank the funding support by EPSRC under the Grant Agreement EP/R001715/1 on "LightForm: Embedding Materials Engineering in Manufacturing with Light Alloys". JDR would like to acknowledge the support of the DSTL/RAEng Chair in Alloys for Extreme Environments.

Supplementary materials

Supplementary material associated with this article can be found, in the online version, at doi:10.1016/j.jma.2023.09.002.

References

- [1] Z. Zeng, N. Stanford, C.H.J. Davies, J.F. Nie, N. Birbilis, Int. Mater. Rev. 64 (1) (2018) 27–62.
- [2] K. Zhang, J.H. Zheng, Z. Shao, C. Pruncu, M. Turski, C. Guerini, J. Jiang, Mater. Des. 184 (2019) 108160.
- [3] M.T. Pérez-Prado, J. Bohlen, S. Yi, D. Letzig, T. Al-Samman, J. Robson, M. Barnett, W. Poole, C. Mendis, S. Agnew, N. Stanford, JOM 72 (7) (2020) 2561–2567.
- [4] K. Zhang, J. Jiang, J. Mater. Res. Technol. 25 (2023) 7454-7459.
- [5] B.Y. Liu, F. Liu, N. Yang, X.B. Zhai, L. Zhang, Y. Yang, B. Li, J. Li, E. Ma, J.F. Nie, Z.W. Shan, Science 365 (6448) (2019) 73–75.
- [6] Z.R. Zeng, Y.M. Zhu, R.L. Liu, S.W. Xu, C.H.J. Davies, J.F. Nie, N. Birbilis, Acta Mater. 160 (2018) 97–108.
- [7] I. Toda-Caraballo, E.I. Galindo-Nava, P.E.J. Rivera-Díaz-del-Castillo, Acta Mater. 75 (2014) 287–296.
- [8] Z. Wu, R. Ahmad, B. Yin, S. Sandlöbes, W.A. Curtin, Science 359 (6374) (2018) 447–452.
- [9] F. Zarandi, S. Yue, Magnesium Sheet; Challenges and Opportunities, Magnesium Alloys-Design, Processing and Properties, InTech, 2011.
- [10] H. Pan, R. Kang, J. Li, Z. Zeng, H. Xie, Q. Huang, C. Yang, Y. Ren, G. Qin, Acta Mater. 186 (2020) 278–290.

- [11] S.Q. Zhu, H.G. Yan, X.Z. Liao, S.J. Moody, G. Sha, Y.Z. Wu, S.P. Ringer, Acta Mater. 82 (2015) 344–355.
- [12] A. Imandoust, C.D. Barrett, A.L. Oppedal, W.R. Whittington, Y. Paudel, H. El Kadiri, Acta Mater. 138 (2017) 27–41.
- [13] K. Huang, R.E. Logé, Mater. Des. 111 (2016) 548-574.
- [14] T. Al-Samman, K.D. Molodov, D.A. Molodov, G. Gottstein, S. Suwas, Acta Mater. 60 (2) (2012) 537–545.
- [15] J.J. Bhattacharyya, S.R. Agnew, G. Muralidharan, Acta Mater. 86 (2015) 80–94
- [16] D. Guan, W.M. Rainforth, J. Gao, J. Sharp, B. Wynne, L. Ma, Acta Mater. 135 (2017) 14–24.
- [17] R. Peng, C. Xu, Y. Li, S. Zhong, X. Cao, Y. Ding, Mater. Res. Lett. 10 (5) (2022) 318–326.
- [18] H. Zhang, X. Bai, M. Hou, L. Wang, Q. Zhang, J. Fan, Y. Wu, H. Dong, B. Xu, Mater. Sci. Eng. A 772 (2020) 138686.
- [19] Q. Ma, B. Li, W.R. Whittington, A.L. Oppedal, P.T. Wang, M.F. Horstemeyer, Acta Mater. 67 (2014) 102–115.
- [20] W.J. Kim, Y.G. Lee, M.J. Lee, J.Y. Wang, Y.B. Park, Scr. Mater. 65 (12) (2011) 1105–1108.
- [21] D. Guan, W.M. Rainforth, L. Ma, B. Wynne, J. Gao, Acta Mater. 126 (2017) 132–144.
- [22] K. Zhang, Z. Shao, C.S. Daniel, M. Turski, C. Pruncu, L. Lang, J. Robson, J. Jiang, Mater. Sci. Eng. A 807 (2021) 140821.
- [23] K. Zhang, J.H. Zheng, Y. Huang, C. Pruncu, J. Jiang, Mater. Des. 193 (2020) 108793.
- [24] F. Kabirian, A.S. Khan, T. Gnäupel-Herlod, Int. J. Plast. 68 (2015) 1-20.
- [25] J. Jain, J. Zou, C.W. Sinclair, W.J. Poole, J. Microsc. 242 (1) (2011) 26–36.
- [26] S.W. Choi, J.W. Won, S. Lee, J.K. Hong, Y.S. Choi, Mater. Sci. Eng. A 738 (2018) 75–80.
- [27] H. Yang, H. Li, H. Sun, Y.H. Zhang, X. Liu, M. Zhan, Y.L. Liu, M.W. Fu, Int. J. Plast. 156 (2022) 103348.

- [28] S. Zhao, R. Zhang, Q. Yu, J. Ell, R.O. Ritchie, A.M. Minor, Science 373 (6561) (2021) 1363–1368.
- [29] G. Han, Y. Noh, U.M. Chaudry, S.H. Park, K. Hamad, T.S. Jun, Mater. Sci. Eng. A 831 (2022) 142189.
- [30] B. Che, L. Lu, J. Zhang, J. Zhang, M. Ma, L. Wang, F. Qi, Mater. Sci. Eng. A 832 (2022) 142475.
- [31] S.H. Park, H.S. Kim, J.H. Bae, C.D. Yim, B.S. You, Scr. Mater. 69 (3) (2013) 250–253.
- [32] G. Mohamed, B. Bacroix, Acta Mater. 48 (13) (2000) 3295-3302.
- [33] S.H. Bae, K.H. Jung, Y.C. Shin, D.J. Yoon, M. Kawasaki, Mater. Charact. 112 (2016) 105–112.
- [34] M. Calcagnotto, D. Ponge, E. Demir, D. Raabe, Mater. Sci. Eng. A 527 (10–11) (2010) 2738–2746.
- [35] S. Yi, J. Bohlen, F. Heinemann, D. Letzig, Acta Mater. 58 (2) (2010) 592–605.
- [36] J. Wang, J.M. Molina-Aldareguía, J. Llorca, Acta Mater. 188 (2020) 215–227.
- [37] J. Jiang, T.B. Britton, A.J. Wilkinson, Acta Mater. 61 (19) (2013) 7227–7239.
- [38] C.W. Su, L. Lu, M.O. Lai, Philos. Mag. 88 (2) (2008) 181–200.
- [39] D. Guan, W.M. Rainforth, J. Gao, L. Ma, B. Wynne, Acta Mater. 145 (2018) 399–412.
- [40] M.R. Barnett, Mater. Sci. Eng. A 464 (1-2) (2007) 8-16.
- [41] K. Zhang, Z. Shao, J. Jiang, Mater. Des. 194 (2020) 108936.
- [42] M.R. Barnett, Z. Keshavarz, A.G. Beer, D. Atwell, Acta Mater. 52 (17) (2004) 5093–5103.
- [43] A. Jain, O. Duygulu, D.W. Brown, C.N. Tomé, S.R. Agnew, Mater. Sci. Eng. A 486 (1–2) (2008) 545–555.
- [44] M.A. Kumar, I.J. Beyerlein, Mater. Sci. Eng. A 771 (2020) 138644.
- [45] K. Wei, R. Hu, D. Yin, L. Xiao, S. Pang, Y. Cao, H. Zhou, Y. Zhao, Y. Zhu, Acta Mater. 206 (2021) 116604.